

Title Page (with Author Details)

Property Analysis of β -Tetragonal Bismite Thin Films: Varied Concentrations and Enhanced Photocatalytic Efficiency

Hella Houda¹, Guettaf Temam Elhachmi¹, Mohammed Althamthami^{*1}, Hachemi Ben
Temam¹, Saâd Rahmane¹

¹*Physics Laboratory of Thin Layers and Applications, Biskra University, BP 145 RP,
Biskra 07000, Algeria*

*Corresponding author. (Mohammed Althamthami)

Tel.: +1 (604) 616 7293

E-mail.: mohammednasser132@gmail.com ; mohammed.althamthami@univ-biskra.dz ; mohammed.althamth1@ucalgary.ca

ORCID.: 0000-0003-1622-9662

Acknowledgements

The authors would like to thank the Algerian Directorate General for Scientific Research and Technological Development-DGRSDT for financial assistance.

Authors wish to thank Mr. Saâd Rahmane and Mr. Brahim Gasmi for his assistance in XRD data acquisition from (LPCMA), University of Biskra, Algeria and Pr. Tibarmacine from the University of Biskra, Algeria.

Manuscript (Without Author Details)

Property Analysis of β -Tetragonal Bismite Thin Films: Varied Concentrations and Enhanced Photocatalytic Efficiency

Abstract

In this study, we thoroughly examine β - Bi_2O_3 thin films as potential photocatalysts. We produced these films using an environmentally friendly Sol Gel method that is also cost-effective. Our research focuses on how different precursor concentrations, ranging from 0.1 M to 0.4 M, affect the photocatalytic performance of these films. We conducted a comprehensive set of tests to analyze various aspects of the films, including their structure, morphology, topography, optical properties, wettability, and photocatalytic capabilities. These tests provided us with a well-rounded understanding of the films' characteristics. To assess their photocatalytic efficiency, we used Methylene Blue (MB) as a contaminant and found that the films, particularly those with a 0.1 M concentration, achieved an impressive 99.9% degradation of MB within four hours. The 0.1 M film had a crystalline size of 39.7 nm, an indirect band gap of 2.99 eV, and a contact angle of 51.37° . Our findings suggest that β - Bi_2O_3 films, especially the 0.1 M variant, have promising potential for treating effluents from complex industrial dye processes. This research marks a significant step in utilizing sustainable materials to address pollution and environmental remediation challenges.

Keywords: Bismuth oxide; Dip coating; photocatalysis; Thin Films; Wettability.

1. Introduction

Organic dyes pose a considerable threat to environmental contamination [1–3]. They exhibit high levels of toxicity and can be hazardous when released into the environment, posing risks to aquatic organisms, humans, plants, and animals [4]. Therefore, it is crucial to implement effective treatment of these textile effluents before their discharge into the environment [5]. Out of the numerous techniques at hand, photocatalytic technology emerges as one of the foremost and highly effective methods for the elimination of organic dyes [6,7].

In this procedure, the degradation of pollutants in water is achieved by utilizing a catalyst composed of semiconductor nanoparticles and a radiation source. Typically, ultraviolet radiation is employed, although certain studies explore the utilization of solar radiation [8], which is the reagent of choice for the process of photocatalysis due to its abundance, low cost, and environmentally friendly nature [9]. Many semiconductors such as face centered ZnO [10], CdS, MoS₂, ZrO₂ [11], and TiO₂, were used for photocatalysis [12]. Among them, Bi₂O₃ nano-structured thin films have been proven to be valuable photo-catalyst [13]. Bismuth oxide has many advantages, including a large energy bandgap ranging from (2 to 3.96 eV) [14], also has a high refractive index and dielectric permittivity [15]. Bi₂O₃ generally exhibits six crystallographic phases viz α -Bi₂O₃ (monoclinic), β - Bi₂O₃ (tetragonal), γ -Bi₂O₃ (body-centered cubic), δ -Bi₂O₃ (face-centered cubic), ϵ -Bi₂O₃ (orthorhombic), and ω -Bi₂O₃ (triclinic) [16].

Moreover, heat of the stable low-temperature polymorph α -Bi₂O₃ results in the formation of the δ -Bi₂O₃ phase at about 730 °C, which, melts at roughly 825 °C. However, two transitions can occur during cooling: δ -Bi₂O₃ to β -Bi₂O₃ at 650 °C or δ -

۲۵ Bi₂O₃ to γ - Bi₂O₃ at 640 °C [17]. A variety of deposition methods are used to produce
۲۶ Bi₂O₃ thin films, including reactive pulsed laser deposition[18], reactive pulsed laser
۲۷ deposition [19], dip coating [20], chemical vapor deposition [21], and hydrothermal
۲۸ synthesis [22]. The dip coating method is one of the low-cost and simple processing
۲۹ methods. It has attractive advantages including a nonhazardous and well suitable for
۳۰ deposition at low temperatures [20].

۳۱ Methylene blue finds extensive usage in various applications, such as chemical
۳۲ indicators, pigments, biological staining, and more, primarily because of its
۳۳ affordability, solubility in water, and strong coloration [23]. This compound possesses
۳۴ an aromatic ring structure that is notably resistant to natural decomposition in water
۳۵ samples [24]. It is crucial to emphasize that the introduction of methylene blue (MB)
۳۶ into the human body can lead to severe nervous system damage [25], resulting in health
۳۷ concerns like eye irritation, breathing difficulties, mental disorientation, vomiting, and
۳۸ excessive perspiration [26].

۳۹ To promote the photocatalytic activity of Bi₂O₃, Wu Xiaohong et al. demonstrated
۴۰ that Bi₂O₃ thin films obtained through a Sol-gel synthesis route and deposited via dip-
۴۱ coating method showed photocatalytic activity in the degradation of Rhodamine B,
۴۲ being this property related to the different temperatures applied during thermal
۴۳ treatment under UV visible irradiation [14]. H. Baqiah et al. studied the Effects of
۴۴ precursor concentration on the microstructural, optical and photoelectrochemical
۴۵ properties of Bi₂O₃ films synthesized by sol-gel method [27]. These studies have not
۴۶ investigated the influence of the precursor concentration of Bi₂O₃ on the photocatalytic
۴۷ performance of MB using the sol-gel with dip-coating method.

48 Within the confines of this manuscript, we have meticulously employed the Sol-gel
49 dip-coating technique to fabricate Bi₂O₃ thin films atop transparent glass substrates.
50 The prime objective of this scholarly endeavor is to delve into the intricate interplay of
51 precursor concentrations (0.1, 0.2, 0.3, and 0.4 M) and their consequential impact on
52 the photonic prowess of the generated samples. This research embarks on an
53 exploration of paramount significance: the measurement of the photocatalytic prowess
54 of these films. Under the radiant of sunlight, their efficacy in the degradation of
55 methylene blue is discerningly examined. To fully grasp the multifaceted attributes of
56 these thin films, analytical tools are meticulously orchestrated. X-ray diffraction
57 (XRD), energy dispersive spectroscopy (EDS), scanning electron microscopy (SEM),
58 UV-VIS spectroscopy, profilometry, and contact angle measurement collectively
59 contribute to unraveling the nuanced characteristics of these films.

60 **2. Materials and methods**

61 *2.1. Preparation of Bi₂O₃ Thin Films*

62 The following technique was used to elaborate nanostructured Bi₂O₃ films: Bi-
63 (NO₃)₃.5H₂O was dissolved in a 48.4 mL nitric acid solution (67.5% purity) with
64 volume ratio [1:8 HNO₃: H₂O]. Then, 4 mL of polyethylene glycol
65 (HO(CH₂CH₂O)₂₀₀H) was added to the solution, followed by 2 g of citric acid; the
66 solution was stirred for 15 min before each addition, and then 0.2 mL of Triton X-100
67 (t-Oct-C₆H₄-(OCH₂CH₂)_x. OH, x=9-10) as a surfactant was added drop by drop. After
68 that, the solution was well stirred for 3h to obtain Sol solution. The sol was heated to
69 60 °C for 90 min to form a gel. A schematic diagram of the sol-gel synthesis was given
70 in **Fig. 1**.

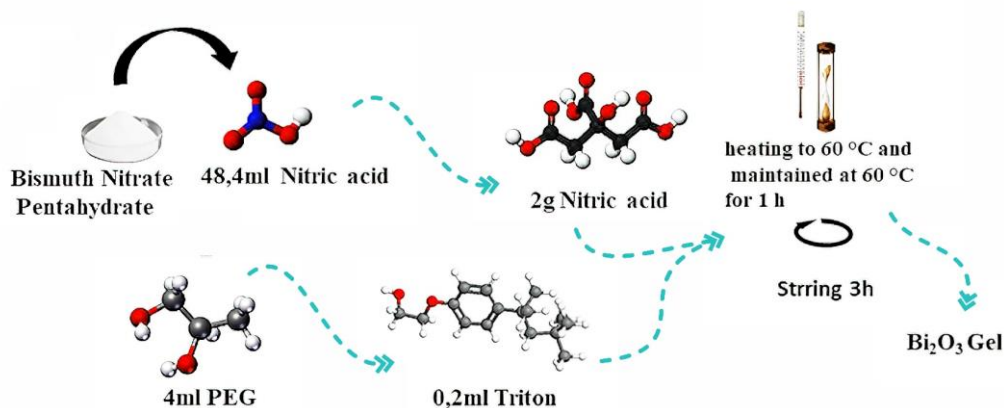


Fig .1. Schematic diagram of Bi_2O_3 preparation by sol-gel synthesis.

The solutions have been deposited on glass substrates (*MICROSCOPE SLIDES, No. 7101*), with dimensions of $(7.5 \times 2.5 \times 0.1 \text{ cm}^3)$. Glass slides were cleaned by ultrasonic cleaning in acetone ($\text{C}_3\text{H}_6\text{O}$) and deionized water for 10 min each, then dried in open air to get well-adhered and smooth films. The weight of glass substrates was measured before and after deposition solutions to measure the thickness of samples using a sensitive balance with four digits (an analytical balance). Following that, the glass substrates were immersed in the solution for 3 min before being withdrawn at 5 cm/min and dried at 110 °C for 10 min to allow organic components to be removed. This process was repeated 10 times. The films were annealed with a heating rate of 5 °C/min for 2 h at 550 °C because the crystallization of bismuth oxides annealed at 550 °C is better than that of bismuth oxides annealed at lower temperatures due to the crystallization of the T (tetragonal) phase of bismuth oxide [28].

2.2. Film characterization:

Bi_2O_3 thin films were characterized by using different physical techniques. Bi_2O_3 crystalline structure of the samples was characterized using grazing-incidence X-ray diffractometry (*D8 Advance*) using $\text{Cu K}\alpha$ irradiation of wavelength 0.15405 nm in the

1.09 2θ range of 20–80°. The crystallite size micro strain and dislocation density of the
1.10 samples determined XRD from spectrum peak broadening.

1.11 The 3D surface topography and surface roughness were assessed using a Tencor P-
1.12 7 mechanical profilometer, which was operated under standard environmental
1.13 conditions at room temperature. This evaluation utilized the 2-bar method with a
1.14 customized filter adjustment, specifically employing a Gaussian filter with a cut-off
1.15 value of 0.800 μm, while addressing edge effects as well.

1.16 The surface morphology and elemental composition were obtained by field emission
1.17 scanning electron microscopy (*JEOL JSM 5800*) combined with energy dispersive X-
1.18 ray (EDX) analysis. The surface roughness of the samples was measured by
1.19 profilometer (*Tencor P-7*).

1.20 Thickness measurement was carried out with the gravimetric weight difference
1.21 method. The transmittance and absorbance spectra were recorded in UV–VIS
1.22 spectrophotometer (*Jasco V-770*) over the 300–900 nm wavelength range. And contact
1.23 angle measurements are performed via the sessile drop method with IC software.

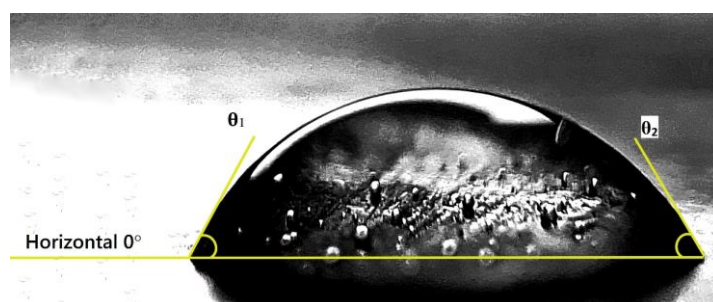
1.24 2.3. Contact angle measurement

1.25 The contact angle measurement reflects the ability of a liquid to spread over a surface
1.26 by wettability. The contact angles of water drop for various bismuth thin films were
1.27 measured at room temperature in ambient atmosphere by homemade method.
1.28 Micropipette (*SCIOLOGEX-iso 9001/13485*) was used to meticulously measure the
1.29 volume of each drop (10 μl), and the distance between micropipette needle and the
1.30 sample was fixed at 7 mm. All contact angles were averaged from five measurements
1.31 with a standard deviation of approximately 5%. The average value of each drop contact

112 angle was determined using IC software. **Fig. 2** describes how the average water droplet
113 contact angle was measured using the following equation:

$$114 \quad \theta_{average} = (\theta_1 + \theta_2)/2 \quad (1)$$

115 Where $\theta_{average}$ is the average angles of θ_1 and θ_2 ($^\circ$), θ_1 is the angle on the left of a
116 water drop ($^\circ$), θ_2 is the angle on the right ($^\circ$) [3,29,30].



117

118 **Fig. 2.** The form denotes how the average value drop's contact angle was calculated.

119 2.4. Preparation of the photocatalytic process for MB

120 The photocatalytic activities of Bi_2O_3 photocatalysts were evaluated by the
121 photodegradation of MB dye under sunlight irradiation at ~ 37 $^\circ\text{C}$. Each film with
122 dimensions of $(4.1*2.5*0.1 \text{ cm}^3)$ was immersed in 100 ml of MB solution (2 mg/L) for
123 1h in the dark to reach the adsorption-desorption equilibrium between Bi_2O_3 particles
124 and MB, then exposed to sunlight with stirring for 4 hours. After that, a 5 ml sample
125 was extracted from each suspension at regular intervals (1h) using syringe filter during
126 the irradiation. After collecting the samples, we recorded UV-vis transmittance of the
127 samples from 300 to 800 nm to measure the degradation of methylene blue [31].

128 3. Results and discussion

129 **Table 1.** Data analysis summary

	Unit	Thin films with different precursor concentrations
--	------	--

		0.1M	0.2M	0.3M	0.4M
<i>Crystallographic dominant Phase</i>		β -Bi ₂ O ₃	β -Bi ₂ O ₃	β -Bi ₂ O ₃	β -Bi ₂ O ₃
<i>Crystal Size</i>	nm	28.6	48.6	41.3	31.8
<i>Surface Roughness (Rq)</i>	nm	18.3	18.4	12.4	8.73
<i>Film Thickness</i>	nm	~40	~73	~83	~115
<i>Transmission in Visible range</i>	%	78	68	68	63
<i>Optical direct Band Gap</i>	eV	3.34	3.41	3.53	3.33
<i>Optical Indirect Band Gap</i>	eV	2.99	3.1	3.24	2.97
<i>Bi Content</i>	wt.%	18.41	22.33	23.27	31.04
<i>O Content</i>	wt.%	34.73	29.88	30.53	27.48
<i>Si Content</i>	wt.%	46.87	47.80	46.20	40.29
<i>Average contact angle</i>	°	51.37±2.1 3	45.57±2.68	67.14±3.6 6	61.61±3.21
<i>MB degradation</i>	%	~99	~96	~95	~93
<i>Constant rate</i>		1.00	0.81	0.76	0.71

۱۳۰

۱۳۱ 3. ۱. X-ray Diffraction

۱۳۲ XRD technique was used to analyze the structure property of the films. The recorded
 ۱۳۳ XRD patterns of the deposited thin films are shown in **Fig. 3(a)**. Moreover, XRD
 ۱۳۴ patterns showed that the common structure is corresponding to Tetragonal (T) phase.
 ۱۳۵ The films (0.1, 0.2, and 0.3 M) mainly consist of monoclinic and tetragonal phases,
 ۱۳۶ which are labeled M and T, respectively. At 0.4 M film, a new peak appeared
 ۱۳۷ corresponding to cubic phase, which has been reported by Wu Xiaohong et al. [14]. The
 ۱۳۸ average crystallite size of the Bi₂O₃ thin films was estimated using the full width at half
 ۱۳۹ maximum (FWHM) from the line broadening of the tetragonal orientation. The average
 ۱۴۰ crystallite sizes were calculated using the Scherrer formula.

$$۱۴۱ \quad D = k \lambda / \beta \cos\theta \quad (2)$$

۱۴۲ where D is the crystal diameter, k is the Scherer constant and is taken equal to 1, λ is
 ۱۴۳ the wavelength of the X-rays, and β is the full width at half maximum (FWHM) of X-
 ۱۴۴ ray diffraction peaks in radians [32]. The average crystallite size of the Bi₂O₃ films

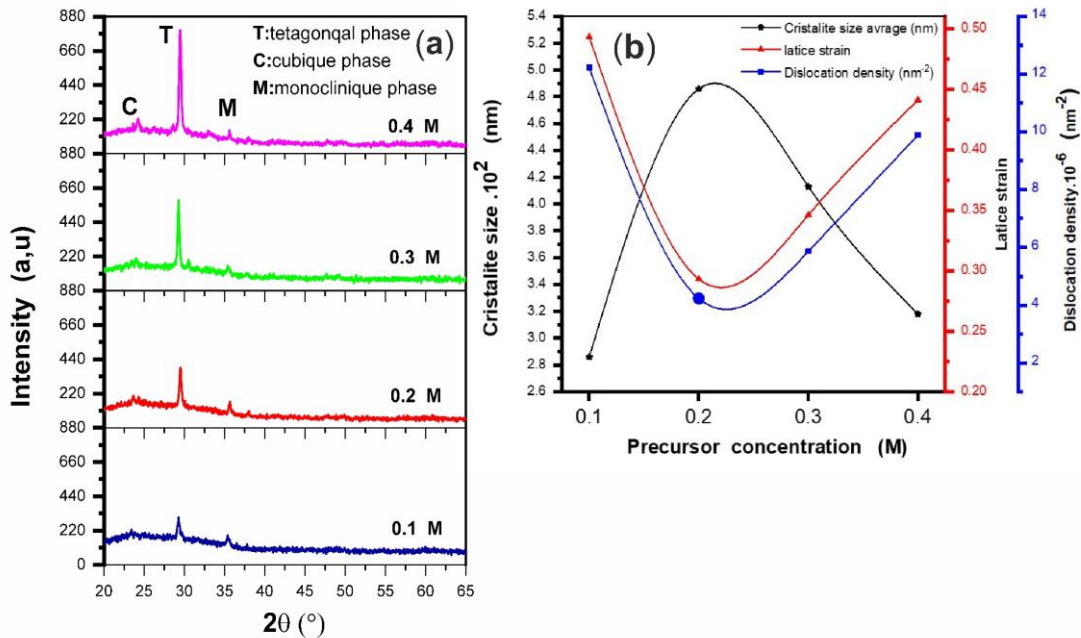
140 prepared by molar precursors of 0.1, 0.2, 0.3, and 0.4 M was found to be 506, 480, 407,
 146 and 360 nm, respectively.

147
$$(\epsilon) = \beta \cos \theta / 4. \pi \quad (3)$$

148 The dislocation density (δ), which represents the defects amount in the sample, is
 149 defined as the length of dislocation lines per unit volume of the crystal [33], and is
 150 calculated using the following relation [34]:

151
$$(\delta) = 1/D^2 \quad (4)$$

152 The structural parameters such as crystallite size, strain ($\epsilon_{\text{average}}$), and dislocation
 153 density (δ_{average}) are listed in **Table 2**. The variation of these parameters was function
 154 of the molar precursor, as shown in **Fig. 3(b)**.



155
 156 **Fig. 3. (a)** XRD spectra of bismuth oxide films prepared by different precursor
 157 concentrations. **(b)** The variation of crystallite size, lattice strain, and dislocation
 158 density as a function of molar concentration of precursor.

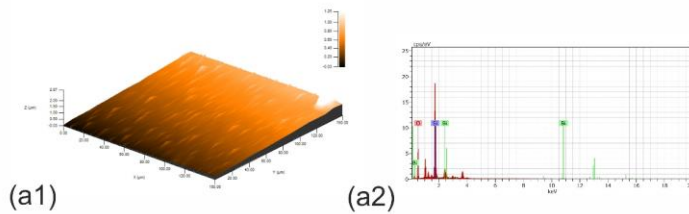
109 It was noticed that the crystallite size varies (from 286 to 486 nm) has inverse relation
 160 with the full width at half maximum FWHM. The small value of (δ) obtained in the
 161 present study confirmed the good crystallinity of the Bi_2O_3 thin films [35]. There is a
 162 direct correlation between dislocation density (from $9.88 \cdot 10^{-6}$ to $1.22 \cdot 10^{-5}$) FWHM as
 163 well as strain, since the more strain creates more dislocations in the structure of the
 164 crystal. This result is in agreement with the previously reported [36].

165 **Tables 2.** The structural parameters of various concentration precursor Bi_2O_3 thin films.

<i>Precursor concentration</i>	<i>Position $2\theta(\text{deg})$</i>	<i>d spacing</i>	<i>FWHM $B_T(\text{deg})$</i>	<i>D(nm)</i>	<i>δ dislocation density (nm^{-2})</i>	<i>ε lattice strain</i>
<i>0.1M</i>	29.28	3.05	0.29	286	$1.22 \cdot 10^{-5}$	0,49
<i>0.2M</i>	29.51	3.06	0.17	486	$4.23 \cdot 10^{-6}$	0,29
<i>0.3M</i>	29.27	3.05	0.20	413	$5.86 \cdot 10^{-6}$	0,34
<i>0.3M</i>	29.43	3.03	0.26	318	$9.88 \cdot 10^{-6}$	0,44

166 3.2. Bi_2O_3 thin films morphological and 3D surface topography

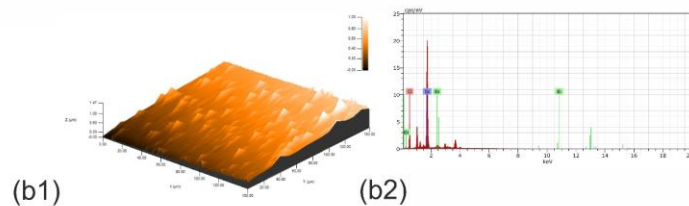
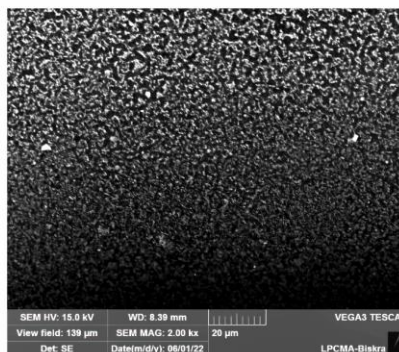
167 The surface morphology of Bi_2O_3 films (from 0.1 to 0.4 M) was carried out using
 168 Scanning Electron Microscope (SEM), as shown in **Fig. 4(a-d)**, respectively. All the
 169 films have irregular island morphology with good overall coverage. **Fig. 4a** shows
 170 isolated islands that are not clustered with each other. When the precursor concentration
 171 is increased, the island grains size increase, this is due to agglomeration in thicker film
 172 resulting grains growth as shown in **Fig. 4(b)** and slightly decreases until the film surface
 173 appears as big grains that are more compact and denser, as shown in **Fig. 4(d)**.



(a1)

(a2)

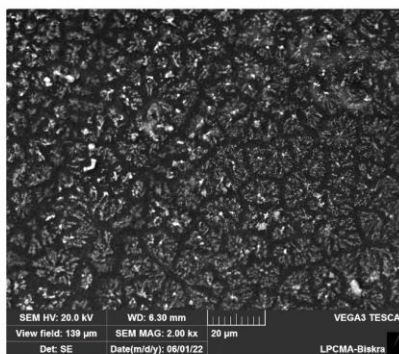
El	AN	Series	unn. C [wt.%]	norm. C [wt.%]	Atom. C [at.%]	Error (1 Sigma) [wt.%]
Si	14	K-series	20.26	50.14	39.78	0.89
O	8	K-series	17.25	42.69	59.45	2.28
Bi	83	L-series	2.90	7.17	0.76	0.21
Total:			40.41	100.00	100.00	



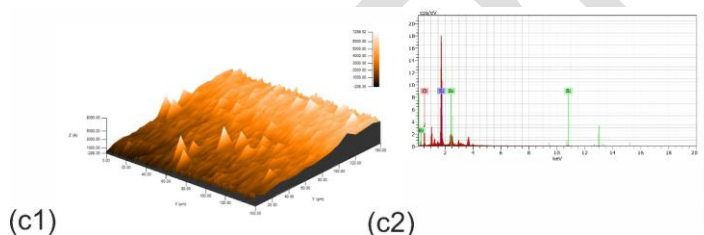
(b1)

(b2)

El	AN	Series	unn. C [wt.%]	norm. C [wt.%]	Atom. C [at.%]	Error (1 Sigma) [wt.%]
Si	14	K-series	22.30	44.44	37.41	0.98
O	8	K-series	20.71	41.27	60.98	2.71
Bi	83	L-series	7.17	14.28	1.62	0.36
Total:			50.18	100.00	100.00	



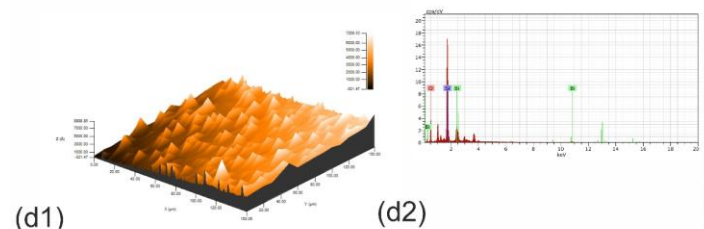
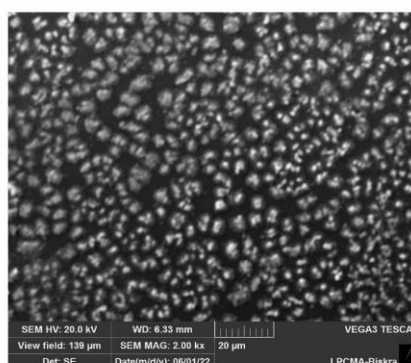
۱۷۵



(c1)

(c2)

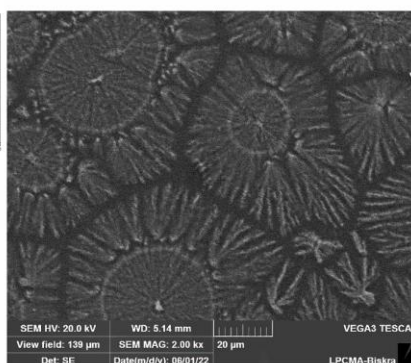
El	AN	Series	unn. C [wt.%]	norm. C [wt.%]	Atom. C [at.%]	Error (1 Sigma) [wt.%]
Si	14	K-series	24.38	42.36	43.49	1.07
O	8	K-series	16.79	29.17	52.58	2.33
Bi	83	L-series	16.39	28.48	3.93	0.69
Total:			57.55	100.00	100.00	



(d1)

(d2)

El	AN	Series	unn. C [wt.%]	norm. C [wt.%]	Atom. C [at.%]	Error (1 Sigma) [wt.%]
Si	14	K-series	23.72	40.18	43.36	1.04
Bi	83	L-series	19.13	32.40	4.70	0.78
O	8	K-series	16.18	27.42	51.94	2.26
Total:			59.03	100.00	100.00	



۱۷۶

177 **Fig. 4.** SEM images and EDS spectrums of Bi₂O₃ films synthesized by the different
 178 precursor concentrations: (a2) 0.1, (b2) 0.2, (c2) 0.3, and (d2) 0.4 M.

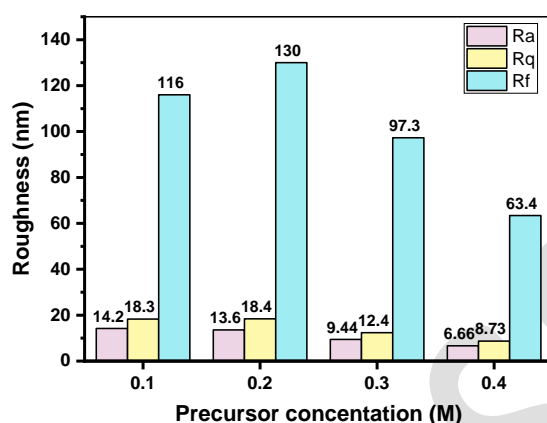
179 The result of cross-sectional SEM images supports the XRD patterns that increasing
 180 the intensity of all diffraction peaks are influenced by the thickness of film. Which is
 181 good agreement with reported [37]. A quantitative analysis of the surface topography
 182 was performed from the data obtained by stylus profilometry. The investigated
 183 parameters include the average roughness, Ra, which is the arithmetic average height
 184 from a mean line over some evaluation length L; the second parameter is the root-mean-
 185 square roughness, Rq, indicating the geometric average height measured from a mean
 186 line within sampling length L; Rt denotes the third parameter and corresponds to the
 187 distance between the highest peak and deepest valley of the profile within the evaluation
 188 length L) [38]. The roughness parameters Ra, Rq, and Rt of different precursor
 189 concentrations are shown in **Table 3.** **Figs. 4** and **5** indicates that Rq values ranged from
 190 8.73 to 18.3 nm, which are slightly higher than Ra (6.66 to 14.2 nm) values, indicating
 191 that the average amplitude from the mean line is higher than the average of peaks and
 192 valleys in the height direction.

193 **Table 3.** 3D surface topography roughness analysis and shape parameters for Bi₂O₃
 194 thin films.

<i>Roughness profile (nm)</i>	<i>Precursor concentration (M)</i>			
<i>Parameters</i>	0.1	0.2	0.3	0.4
<i>Rt (nm)</i>	116	130	97.3	63.4
<i>Rq (nm)</i>	18.3	18.4	12.4	8.73
<i>Ra (nm)</i>	14.2	13.6	9.44	6.66

195 The highest roughness values (18.4 and 18.3 nm) correspond to the compounds
 196 deposited with 0.2 and 0.1M films, which increase the photocatalytic efficiency. The

197 lower roughness values were 9.44 nm and 6.66 nm, corresponding to 0.3 and 0.4 M
198 films. Larger surface grains of prepared films engendered a rougher surface feature.
199 Similarly, a substantially increased surface grain size, as reported in the ZnO film [39].



200

201 **Fig. 5.** The roughness parameters Ra, Rq, and Rt of Bi₂O₃ films prepared at various
202 molar concentrations.

203 3.3. Bi₂O₃ thin films EDS analysis patterns

204 The EDS compositional analysis of bismuth thin films at different precursor
205 concentrations is shown in **Fig. 4(a–d)**, respectively. This spectrum confirms the
206 presence of Bi and O elements in the films. The results also indicate the presence of Si,
207 which is attributed to the substrate glass used [40]. The Bi content increases (from 18.48
208 to 27.48 wt. %) as the molar concentration increases from 0.1 to 0.4 M, which is
209 attributed to rise in its atomic percentage. Whereas the decrease in oxygen content
210 (from 34.73 to 27.48 wt.%) could be due to the chemisorbed oxygen from the
211 atmospheric air [41].

212 3.4. Spectral analysis UV-visible

۲۱۳ The optical properties of Bi₂O₃ thin films prepared by using various precursor
 ۲۱۴ concentrations were studied by UV–visible spectrophotometer in the range of 300–900
 ۲۱۵ nm at room temperature, is depicted in **Fig. 7(a)**. As noticed, the transmittance increases
 ۲۱۶ with increasing wavelength, and its average value in the visible region of the spectrum
 ۲۱۷ is (78, 67.66%, 67.68%, and 63%); in the ultraviolet region, it is (51, 32, 34%, and
 ۲۱۸ 18%), with rising precursor concentrations (from 0.1 to 0.4 M), respectively. The
 ۲۱۹ transmittance can be associated with the values of grain size, RMS, porosity, and
 ۲۲۰ thickness of the films. It is generally expected that increased thickness and surface
 ۲۲۱ roughness lead to reduced transmittance, while decreasing porosity and grain size
 ۲۲۲ decrease transmittance [42]. The gravimetric weight differential method (weight
 ۲۲۳ increase method) was used to determine the thickness of the Bi₂O₃ films.

$$۲۲۴ \quad D = \Delta m / A \cdot \rho \quad (4)$$

۲۲۵ Where Δm is the mass difference in grams, A is the area of deposited films in cm², and
 ۲۲۶ ρ is the density of the deposited material (Bi₂O₃= 9.17 g/cm³) [43]. **Fig. 7(d)** shows the
 ۲۲۷ average thickness variation as a function of concentration precursor values. The film
 ۲۲۸ thickness increased (from 40 to 115 nm) as the precursor concentration increased (from
 ۲۲۹ 0.1 to 0.4 M); this is due to the high viscosity of the solution. The absorption coefficient
 ۲۳۰ α of the mentioned films was obtained via the following equation:

$$۲۳۱ \quad \alpha = \ln I_0/I \cdot 1/d \quad (5)$$

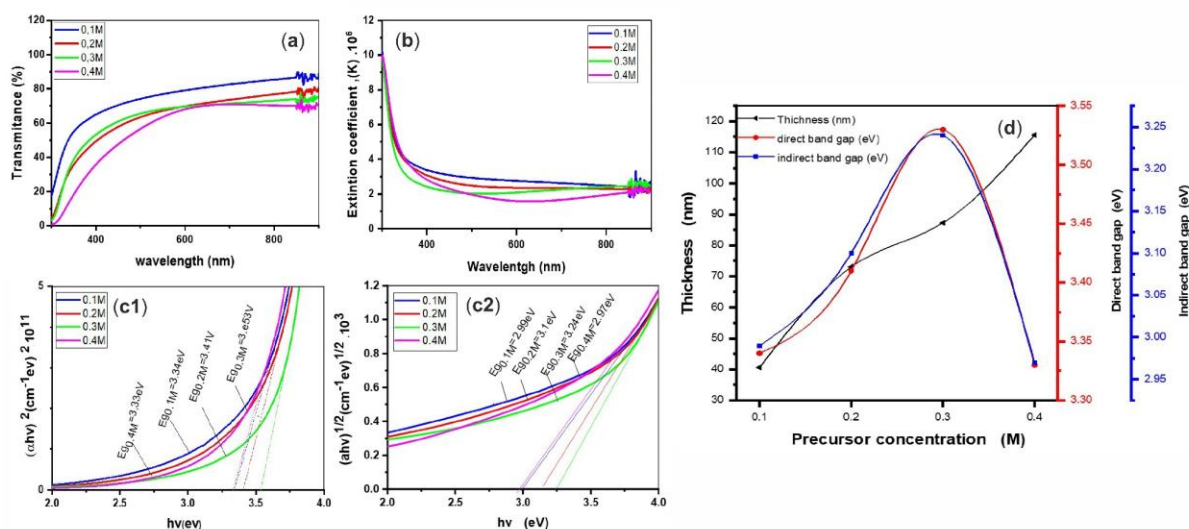
۲۳۲ Where, d is film thickness, and I_0/I is the ratio of incident beam intensity to emergent
 ۲۳۳ beam [17][30]. Band gap values are calculated from absorption spectra, and the method
 ۲۳۴ was described in previous literature [45]. The data were analyzed using the following
 ۲۳۵ classical relationship for optical transitions:

۲۳۶
$$(\alpha h\nu)^2 = A(h\nu - E_g)^n \quad (6)$$

۲۳۷ Where α , h , ν , E_g , and A are the absorption coefficient, Planck constant, light
۲۳۸ frequency, band gap energy, and a is constant, respectively [46,47]. There are two types
۲۳۹ of band gaps: direct band gaps and indirect band gaps; an electron can emit a photon
۲۴۰ directly in a direct band gap but not in an indirect band gap because the electron must
۲۴۱ pass through an intermediate state to transfer momentum to the crystal lattice [46]. The
۲۴۲ estimated direct and indirect transition band-gap values are demonstrated in **Fig. 7(c1,**
۲۴۳ **c2)**, which show the variation of direct and indirect band-gap values with different
۲۴۴ precursor concentrations. Both the direct and indirect band gap energies increased as
۲۴۵ the precursor concentration increased from 0.1 to 0.3 M, and then they decreased at
۲۴۶ 0.4M, these results were related to the transmittance of the films. The direct and indirect
۲۴۷ band gaps of the Bi_2O_3 films with precursor concentrations of 0.1 and 0.4 M were the
۲۴۸ lowest; on the other hand, 0.2 and 0.3M are the highest. The extinction coefficient (k)
۲۴۹ can be obtained from the relation [48] :

۲۵۰
$$K = \alpha\lambda / 4.\pi \quad (7)$$

۲۵۱ The variation of extinction coefficient with wavelength was shown in **Fig. 7(b)**. The
۲۵۲ extinction coefficient was high in the 300–400 nm range and low in the 400–900 nm
۲۵۳ range. The rise in the extinction coefficient is directly related to absorption of light.

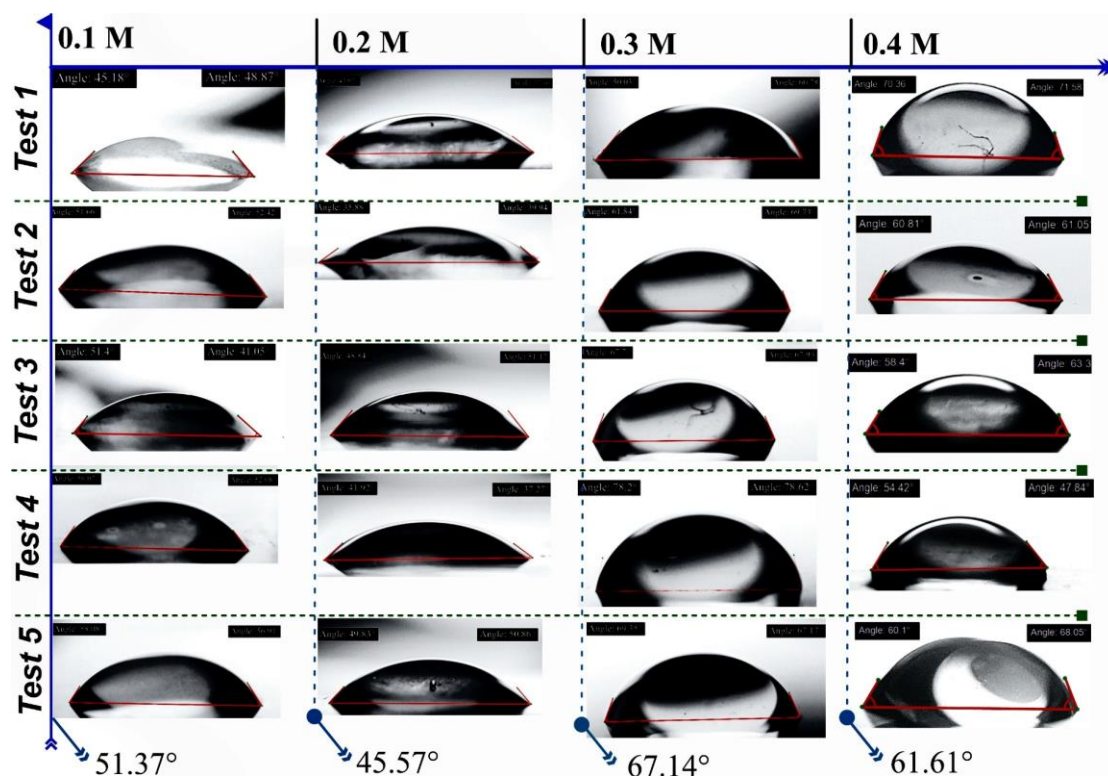


۲۵۴

۲۵۵ **Fig. 7.** (a) Optical transmittance spectrum of Bi_2O_3 synthesized by the different
 ۲۵۶ precursor concentrations. (b) Variation of extinction coefficient (k) versus wavelength
 ۲۵۷ with various molar concentrations. (c1) Direct and (c2) indirect band gap of the Bi_2O_3
 ۲۵۸ films. (d) Variation of thickness and band gap with different precursor concentrations.

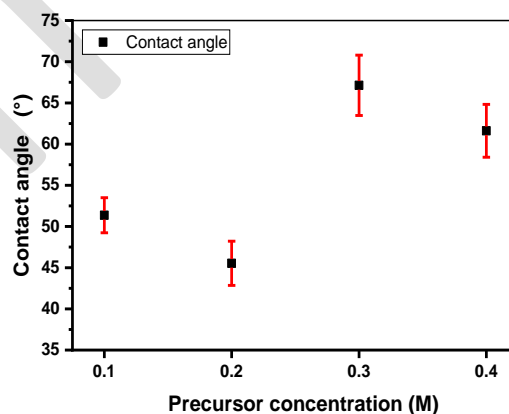
۲۵۹ 3.5. Wettability analysis

۲۶۰ The wetting behavior of a solid surface in contact with water is determined by the
 ۲۶۱ interfacial tension between the surrounding medium (usually air) and water. When a
 ۲۶۲ surface exhibits high wettability, it tends to have a low contact angle, indicating that it
 ۲۶۳ is hydrophilic in nature and readily interacts with water. Conversely, when the
 ۲۶۴ wettability is low, the contact angle is high, suggesting that the surface is hydrophobic
 ۲۶۵ and repels water [43,49]. In the case of Bi_2O_3 films, as depicted in **Fig. 8**, water contact
 ۲۶۶ angle measurements were conducted.



۲۷۱ **Fig. 8.** Contact angles measurements images of Bi_2O_3 thin films.

۲۶۹ The average contact angles for the samples with concentrations of 0.1 M, 0.2 M, 0.3
 ۲۷۰ M, and 0.4 M were found to be 51.37°, 45.57°, 67.14°, and 61.61°, respectively, as
 ۲۷۱ illustrated in **Fig. 9**.



۲۷۲ **Fig. 9.** Average contact angles of distilled water (H_2O) on the Bi_2O_3 substrates.

۲۷۳ These results indicate that all the films exhibit a hydrophilic nature, implying that
 ۲۷۴ they have a strong affinity for water. This hydrophilic property facilitates the interaction
 ۲۷۵

of the photocatalysts with contaminants in water, leading to improved degradation performance [50].

3.6. The photocatalytic efficiency

The photocatalytic efficiency of Bi₂O₃ thin films synthesized with variable precursor concentrations was evaluated by MB (2 ppm) photobleaching in an aqueous solution.

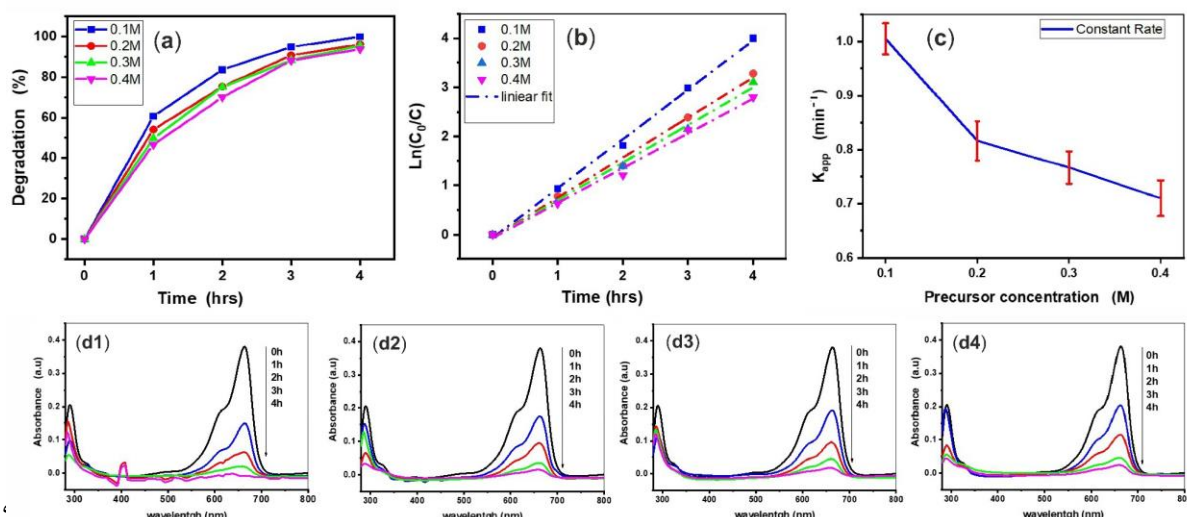
Table. 4 shows the variation of temperature, wind, and humidity for each hour. **Fig.**

10(a) shows the time-dependent visible light photocatalysis of thin films (0.1, 0.2, 0.3, 0.4 M) which decomposes the MB dye with a total exposure time of 4 h.

Table 4. Change in temperature, wind, humidity, and the amount of solar radiation per hour in the BM degradation test (Biskra, Algeria) on 20 April 2021.

<i>Time (h)</i>	0	1	2	3	4
<i>Day temp (C^o)</i>	25	26	27	27	28
<i>Wind speed (km/h)</i>	12	11	10	9	9
<i>Humidity (%)</i>	41	40	38	37	35
<i>Radiation amount</i>	moderate				

The absorbance edge of MB dye at 664 nm was decreased with increasing sunlight irradiation time.



۲۸۶

۲۹۰ **Fig. 10.** (a) The degradation rate of MB dye by Bi₂O₃ thin films. (b) Photocatalytic
 ۲۹۱ kinetics for the all Bi₂O₃ thin films. (c) Effects of varying precursor concentrations of
 ۲۹۲ Bi₂O₃ thin films on MB removal under irradiation time. Absorbance spectra of the
 ۲۹۳ MB solutions by Bi₂O₃ thin films prepared with different precursor concentrations:
 ۲۹۴ (d1) 0.1, (d2) 0.2, (d3) 0.3, and (d4) 0.4 M.

۲۹۵ The degradation rate of MB dye is revealed in the presence of thin films as a catalyst.

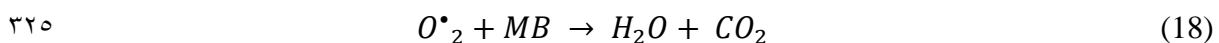
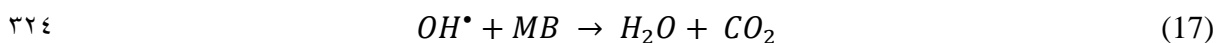
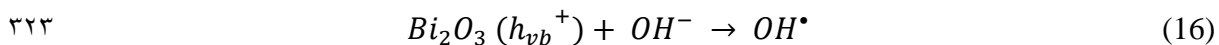
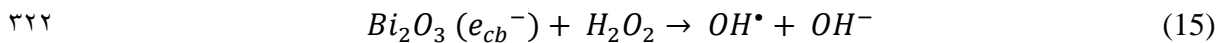
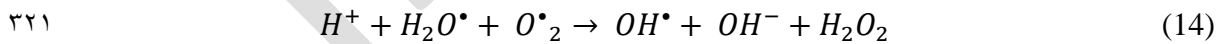
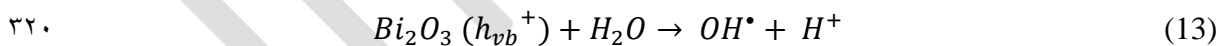
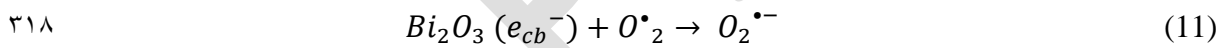
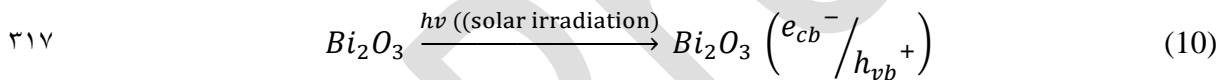
۲۹۶ The following equation was used to calculate the photo degradation rate: [51]

$$D = A_0 - A_t/A_0 * 100 \% \quad (8)$$

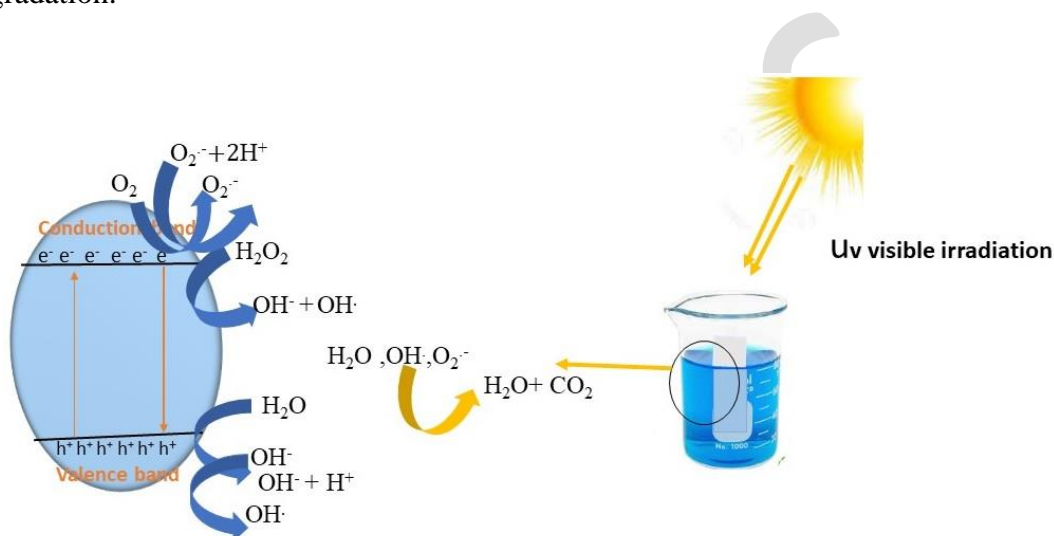
۲۹۸ Where A_0 is the initial absorbance at time $t = 0$ h, A_t is the absorbance after time t . The
 ۲۹۹ absorbance of MB dye over the Bi₂O₃ thin films under sun irradiation for 4 h is shown
 ۳۰۰ in **Fig. 10(d(1, 2, 3, and 4))**. It was observed that after 2h the relative amounts of MB
 ۳۰۱ decomposed by photocatalysis were 47.09, 49.47, 53.97, and 83.60 % when Bi₂O₃
 ۳۰۲ synthesized at 0.1, 0.3, 0.4, and 0.5 M was used as photocatalyst, respectively. Bi₂O₃
 ۳۰۳ thin films prepared at 0.1M have the highest photocatalytic efficiency among all
 ۳۰۴ samples, with 99.9 % at 4 h irradiation time. The kinetics of the photocatalytic
 ۳۰۵ degradation process can be generally explained by the L-H kinetic mode. [52]

$$\ln(C_0/C_t) = kt \quad (9)$$

Where C_0 is the concentration at time t_0 , C_t is the concentration at particular irradiation time, and k is the apparent pseudo-first-order rate constant (min^{-1}). The apparent rate constant (k) was successfully calculated from the slopes of the straight line obtained from the plot of natural logarithm by plotting the $\ln(C_0/C_t)$ vs irradiation time [31]. The plot of $-\ln(C/C_0)$ as a function of irradiation time for films Bi_2O_3 prepared by different precursor molarities is presented in **Fig. 10(b)**. **Fig. 10(c)** shows kinetic rate of degradation of the dye solutions with increasing amounts of bismuth precursor. As observed, the highest kinetic rate decreases with increasing molar precursors, so the highest rate 99.9% is exhibited by 0.1 M. The following equations outline the photocatalytic attributes of Bi_2O_3 films within an MB solution under sunlight [53–55]:



۳۲۶ When bismuth oxide is activated with visible light ($\lambda \geq 420$ nm), electrons are promoted
 ۳۲۷ from the valence band to the conduction band, generating an electron/hole pair (e⁻/h⁺).
 ۳۲۸ (Eq. (10)) which are strong oxidizing and reducing agents, as shown in **Fig. 11** [56].
 ۳۲۹ **Table 5** presents a thorough comparative examination between the current study and
 ۳۳۰ various other research papers that have incorporated thin films and powders as a pivotal
 ۳۳۱ element in their investigations assessing the efficacy of photocatalysts in organic dye
 ۳۳۲ degradation.



۳۳۳
 ۳۳۴ **Fig. 11.** Illustrates the photocatalytic mechanisms of Bi₂O₃ films for MB degradation
 ۳۳۵ under sunlight irradiation.

۳۳۶ The photo-induced holes are powerful oxidizers because of their attraction for
 ۳۳۷ electrons. They oxidize the adsorbed water molecule or hydroxide ion to produce
 ۳۳۸ hydroxyl radicals (**Eq. 13**). On the other hand, the electron from the photoexcitation
 ۳۳۹ attacks the oxygen (**Eq. 11**), it can be reduced to the different oxygen activated species
 ۳۴۰ (**Eq. 11**), Then all these highly oxidizing species ($-\text{OH}$, $\bullet\text{OH}$, H_2O_2 , etc.) are capable
 ۳۴۱ of oxidizing organic molecules, such as MB into simpler molecules such as CO_2 , H_2O
 ۳۴۲ [57,58].

۳۴۳ **Table 5.** Illustrates a comparison between the photocatalytic efficiency of organic dye
 ۳۴۴ degradation observed in this investigation and findings from other studies.

<i>materials</i>	<i>Dye type and concentration</i>	<i>Technique type</i>	<i>Degradation (%)</i>	<i>Time (min)</i>	<i>Irradiation Source</i>	<i>Reference</i>
β -Bi ₂ O ₃ (0.1M), Thin film	Methylene blue, 0.002 g/l	Dip-coating (glass Substrate)	~99	240	Visible light	Current study
β -Bi ₂ O ₃ , Thin film	Methylene blue, 10 ⁻⁶ mol/l	Spin-coating Deposition (Pt-coated silicon substrates)	~100	1440	Solar lamp (Ultra-Vitalux 300 W, Osram)	[59]
β -Bi ₂ O ₃ , Powder	RhB, 5 mg/L	Situ chemical transformation method	~7	25	Xe lamp (350 W)	[60]
BiOBr, Powder	RhB, 5 mg/L	Situ chemical transformation method	~30	25	Xe lamp (350 W)	[60]
Co ₃ O ₄ (Co-3), Thin film	Methylene orange, 0.01 g/l	Nebulizer spray (glass and FTO Substrate)	~57	180	Tungsten Halogen lamp of 300 W (1 > 400 nm)	[61]
Co ₃ O ₄ (withdrawn speed of 5 mm/s), Thin film	Methylene blue, 0.002 g/l	Dip-coating (glass Substrate)	~77	240	Visible light	[62]
CuO/ZnO (simple A), Thin film	Methylene blue, 0.005 g/l	Spin-coating with Glass Substrate	~44	120	Xe lamp of 150 W	[63]
ZnO, Thin film	Methylene blue, 0.003 g/l	Spraying (glass Substrate)	~80	360	Visible light	[64]
CoTiO ₃ /Co ₃ O ₄ , Thin film	Indo Light Blue, 0.01 g/l	Doctor blade and spin coating (glass Substrate)	~29	60	Hg lamp of 250 W	[65]
Cu:Co (30:70), Thin film	Methylene blue, 0.003 g/l	Dip-coating (glass Substrate)	~49	240	Visible light	[7]

۳۴۵

۳۴۶ **4. Conclusion**

۳۴۷ In this study, Bi₂O₃ films are deposited by sol-gel technique. The structural,
۳۴۸ morphological, optical, and photocatalytic properties of Bi₂O₃ thin films were
۳۴۹ investigated as a function of precursor concentrations. The films are polycrystalline
۳۵۰ with tetragonal structure peak as a preferred orientation. The crystallite size of Bi₂O₃
۳۵۱ films was not gradually affected by the change in precursor concentration or film
۳۵۲ thickness. The morphology of the Bi₂O₃ surface indicates irregular and good overall
۳۵۳ coverage, which increase with increasing molar precursor concentration, which is
۳۵۴ supported by Rq area roughness of the sample. The optical spectrum shows that the
۳۵۵ transmission increases with decreasing precursor concentration, and the maximum
۳۵۶ average value of about 78 % in the visible region is observed for film prepared with 0.1
۳۵۷ M. The direct band-gap values varied between 3.33 and 3.53 eV, and the direct band
۳۵۸ gap varied between 2.97 - 3.24 eV when the precursor concentration was from 0.1 to
۳۵۹ 0.4 M. The average contact angles. Measurements proved the hydrophilic nature of the
۳۶۰ films as contact angle between 51.37° and 61.61°. The degradation of MB decreases
۳۶۱ with the increase in precursor concentration, and the kinetic rate of degradation and
۳۶۲ degradation rate also have the highest values among all the thin films. Thus, the Bi₂O₃
۳۶۳ thin film of 0.1M shows the fastest apparent photocatalytic reaction rate MB, at 99.9%,
۳۶۴ corresponding to 39.7 nm crystal size, 2.01 eV band gap energy, 55 nm surface
۳۶۵ roughness, and 51.37° contact angle. From the above results, it can be concluded that
۳۶۶ this Bismuth oxide film is a good photocatalyst for water purification.

۳۶۷ **Declarations**

۳۶۸ **Competing interests**

۳۶۹ The authors report that there are no interests of a financial or personal nature in this
۳۷۰ work.

۳۷۱ **Ethical approval**

۳۷۲ Not applicable.

۳۷۳ **Informed consent**

۳۷۴ Not applicable.

۳۷۵ **Authors' contributions**

۳۷۶ All of the authors have studied this work.

۳۷۷ **Funding**

۳۷۸ The authors have reported that they did not receive any funding.

۳۷۹ **Availability of data and materials**

۳۸۰ The statement regarding the datasets used in this work can be accessed through the
۳۸۱ corresponding author.

۳۸۲ **References**

- ۳۸۳ 1. Kiwaan, H. A., Atwee, T. M., Azab, E. A., El-Bindary, A. A., "Photocatalytic degradation
۳۸۴ of organic dyes in the presence of nanostructured titanium dioxide." *J. Mol. Struct.*,
۳۸۵ 2020, 1200, 115-127.
- ۳۸۶ 2. Gamal Hasan, G., Khelef, A., Chaabia, N., Ali Mohammed, H., Laid Tedjani, M.,
۳۸۷ Althamthami, M., "Fabrication and characterization of NFMA/FTO electrochemical
۳۸۸ thin film by electrodeposition and immersion techniques: An effective detector for
۳۸۹ H₂O₂ and sunlight-driven MB degradation." *J. Photochem. Photobiol. A Chem.*, 2023,
۳۹۰ 445, 112-115.
- ۳۹۱ 3. Hasan, G. G., Mohammed, H. A., Althamthami, M., Khelef, A., Laouini, S. E.,
۳۹۲ Meneceur, S., "Synergistic effect of novel biosynthesis SnO₂@Fe₃O₄ nanocomposite:

- ۳۹۳ A comprehensive study of its photocatalytic of Dyes & antibiotics, antibacterial, and
۳۹۴ antimutagenic activities." *J. Photochem. Photobiol. A Chem.*, 2023, 443, 114-874.
- ۳۹۵ 4. Omidvar, A., Jaleh, B., Nasrollahzadeh, M., "Preparation of the GO/Pd nanocomposite
۳۹۶ and its application for the degradation of organic dyes in water." *J. Colloid Interface*
۳۹۷ *Sci.*, 2017, 496, 44–50.
- ۳۹۸ 5. Nuengmatcha, P., Porrawatkul, P., Chanthai, S., Sricharoen, P., Limchoowong, N.,
۳۹۹ "Enhanced photocatalytic degradation of methylene blue using
۴۰۰ Fe₂O₃/graphene/CuO nanocomposites under visible light." *J. Environ. Chem. Eng.*,
۴۰۱ 2019, 7, 103-438.
- ۴۰۲ 6. Yang, L., Chen, C., Hu, Y., Wei, F., Cui, J., Zhao, Y., Xu, X., Chen, X., Sun, D., "Three-
۴۰۳ dimensional bacterial cellulose/polydopamine/TiO₂ nanocomposite membrane with
۴۰۴ enhanced adsorption and photocatalytic degradation for dyes under ultraviolet-
۴۰۵ visible irradiation." *J. Colloid Interface Sci.*, 2020, 562, 21–28.
- ۴۰۶ 7. Althamthami, M., Elhachmi, G. T., Ben Temam, H., Hasan, G. G., Rahmane, S., Gasmii,
۴۰۷ B., "Effect of Different Cu:Co Film Concentrations on Photocatalytic Reactions of
۴۰۸ Ethanol, MB, AMX, and Cr(VI): A Study of Film Properties & Effects of Photooxidation."
۴۰۹ *J. Environ. Chem. Eng.*, 2023, 111-247.
- ۴۱۰ 8. Reddy, C. V., Reddy, I. N., Harish, V. V. N., Reddy, K. R., Shetti, N. P., Shim, J.,
۴۱۱ Aminabhavi, T. M., "Efficient removal of toxic organic dyes and photoelectrochemical
۴۱۲ properties of iron-doped zirconia nanoparticles." *Chemosphere*, 2020, 239, 124-766.
- ۴۱۳ 9. Akhtar, J., Tahir, M. B., Sagir, M., Bamufleh, H. S., "Improved photocatalytic
۴۱۴ performance of Gd and Nd co-doped ZnO nanorods for the degradation of methylene
۴۱۵ blue." *Ceram. Int.*, 2020, 46, 11955–11961.
- ۴۱۶ 10. Kumari, V., Mittal, A., Jindal, J., Yadav, S., Kumar, N., "S-, N- and C-doped ZnO as
۴۱۷ semiconductor photocatalysts: A review." *Front Mater Sci.*, 2019, 13.
- ۴۱۸ 11. Kabra, K., Chaudhary, R., Sawhney, R. L., "Treatment of hazardous organic and
۴۱۹ inorganic compounds through aqueous-phase photocatalysis: A review." *Ind. Eng.*
۴۲۰ *Chem. Res.*, 2004, 43, 7683–7696.
- ۴۲۱ 12. Soares, L., Alves, A., "Photocatalytic properties of TiO₂ and TiO₂/WO₃ films applied
۴۲۲ as semiconductors in heterogeneous photocatalysis." *Mater. Lett.*, 2018, 211, 339–
۴۲۳ 342.
- ۴۲۴ 13. Li, J. Z., Zhong, J. B., Zeng, J., Feng, F. M., He, J. J., "Improved photocatalytic activity of
۴۲۵ dysprosium-doped Bi₂O₃ prepared by sol-gel method." *Mater. Sci. Semicond.*
۴۲۶ *Process.*, 2013, 16, 379–384.
- ۴۲۷ 14. Xiaohong, W., Wei, Q., Weidong, H., "Thin bismuth oxide films prepared through the
۴۲۸ sol – gel method as photocatalyst." 2007, 261, 167–171.

15. Orozco-Hernández, G., Olaya-Flórez, J., Pineda-Vargas, C., Alfonso, J. E., Restrepo-Parra, E., "Structural, chemical and electrochemical studies of bismuth oxide thin films growth via Unbalanced Magnetron Sputtering." *Surfaces and Interfaces*, 2020, 21, 100-627.
16. Dev, B. C., Babu, M. H., Podder, J., Sagadevan, S., Zubair, A., "Low temperature synthesis of α - and β -phase Bi₂O₃ thin film via B doping: tailoring optical band gap and n- to p-type Bi₂O₃." *J.of Mater. Sci.: Mater. in Ele.*, 2019, 30, 15670–15682.
17. Dapčević, A., Poleti, D., Rogan, J., Radojković, A., Radović, M., Branković, G., "A new electrolyte based on Tm³⁺-doped δ -Bi₂O₃-type phase with enhanced conductivity." *Sol. Sta. Ion.*, 2015, 280, 18–23.
18. Fan, H. T., Pan, S. S., Teng, X. M., Ye, C., Li, G. H., Zhang, L. D., " δ -Bi₂O₃ thin films prepared by reactive sputtering: Fabrication and characterization." *Thin Solid Films*, 2006, 513, 142–147.
19. Zhu, B. L., Zhao, X. Z., "Study on structure and optical properties of Bi₂O₃ thin films prepared by reactive pulsed laser deposition." *Opt. Mater. (Amst.)*, 2006, 29, 192–198.
20. Hettal, S., Ouahab, A., Rahmane, S., Benmessaoud, O., Sayad, M., "Effect of the Number of Dips on the Properties of Copper Oxide Thin Films Deposited by Sol-Gel Dip-Coating Technique." *Iranian Journal of Materials Science and Engineering*, 2022, 19, 1–8.
21. Sun, Z., Oka, D., Fukumura, T., "Epitaxial Growth of β -Bi₂O₃ Thin Films and Particles with Mist Chemical Vapor Deposition." *Cryst. Growth Des.*, 2019, 19, 7170–7174.
22. Wu, S., Fang, J., Xu, W., Cen, C., "Hydrothermal synthesis, characterization of visible-light-driven α -Bi₂O₃ enhanced by Pr³⁺ doping." *Journal of Chemical Technology and Biotechnology*, 2013, 88, 1828–1835.
23. Tong, Y., Jiang, B., Chen, X., Ren, X., Lu, J., Ding, L., "Synergistic degradation of methylene blue by laser cavitation and activated carbon fiber." *Opt. Laser Technol.*, 2022, 155, 108-417.
24. Chen, M. L., Li, S. S., Wen, L., Xu, Z., Li, H. H., Ding, L., Cheng, Y. H., "Exploration of double Z-type ternary composite long-afterglow/graphitic carbon nitride@metal-organic framework for photocatalytic degradation of methylene blue." *J. Colloid Interface Sci.*, 2023, 629, 409–421.
25. Arif, M., Liu, G., Yousaf, B., Ahmed, R., Irshad, S., Ashraf, A., Zia-ur-Rehman, M., Rashid, M. S., "Synthesis, characteristics and mechanistic insight into the clays and clay minerals-biochar surface interactions for contaminants removal-A review." *J. Clean Prod.*, 2021, 310, 127-548.

26. El-Ghobashy, M. A., Salem, I. A., El-Dahrawy, W. M., Salem, M. A., "Fabrication of α -MnO₂/Fe-Mn binary oxide nanocomposite as an efficient adsorbent for the removal of methylene blue from wastewater." *J. Mol. Struct.*, 2023, 1272, 118-134.
27. Baqiah, H., Talib, Z. A., Liew, J. Y. C., Shaari, A. H., Zainal, Z., F, L. M., "Effects of precursor concentration on the microstructural, optical and photoelectrochemical properties of Bi₂O₃ films synthesized by sol-gel method." *Optik. (Stuttg.)*, 2020, 206.
28. Weidong, H., Wei, Q., Xiaohong, W., Hailong, N., "Thin bismuth oxide films prepared through the sol – gel method." 2007, 61, 4100–4102.
29. Althamthami, M., Guettaf Temam, E., Ben Temam, H., Hasan, G. G., Malfi, N., "Influence of hole-scavenger and different withdrawn speeds on photocatalytic activity of Co₃O₄ thin films under sunlight irradiation." *Ceram. Int.*, 2022, 48, 31570–31578.
30. Althamthami, M., Guettaf Temam, E., Temam, H. Ben, Saad, R., Hasan, G. G., "Improved photocatalytic activity under the sunlight of high transparent hydrophilic Bi-doped TiO₂ thin-films." *J. Photochem. Photobiol. A Chem.*, 2023, 443, 114-818.
31. Raza, W., Bahnemann, D., Muneer, M., "A green approach for degradation of organic pollutants using rare earth metal doped bismuth oxide." *Catal. Today*, 2018, 300, 89–98.
32. Jadhav, C. H., Pagare, P. K., Inamdar, K. K., Kadam, L. D., "Preparation of Bismuth Oxide Thin Films by Spray Pyrolysis Method and Its Characterizations." *Macromol. Symp.*, 2019, 387, 1–3.
33. Seid, E. T., Dejene, F. B., Urgessa, Z. N., Botha, J. R., "Refluxed sol–gel synthesized ZnO nanopowder with variable zinc precursor concentrations." *Appl. Phys. A Mater. Sci. Process*, 2018, 124, 1–13.
34. Ravishankar, S., Balu, A. R., Anbarasi, M., Nagarethinam, V. S., "Influence of precursor molar concentration on the structural, morphological, optical and electrical properties of PbS thin films deposited by spray pyrolysis technique using perfume atomizer." *Optik. (Stuttg.)*, 2015, 126, 2550–2555.
35. Kamble, D. L., Harale, N. S., Patil, V. L., Patil, P. S., Kadam, L. D., "Characterization and NO₂ gas sensing properties of spray pyrolyzed SnO₂ thin films." *J. Anal. Appl. Pyrolysis.*, 2017, 127, 38–46.
36. Seid, E. T., Dejene, F. B., Urgessa, Z. N., Botha, J. R., "Refluxed sol–gel synthesized ZnO nanopowder with variable zinc precursor concentrations." *Appl. Phys. A Mater. Sci. Process*, 2018, 124, 1–13.
37. Aryanto, D., Jannah, W. N., Masturi, Sudiro, T., Wismogroho, A. S., Sebayang, P., Sugianto, Marwoto, P., "Preparation and structural characterization of ZnO thin films by sol-gel method." *J. Phys. Conf. Ser.*, 2017, 817, 012-025.

- 0.2 38. Pérez-González, M., Tomás, S. A., Santoyo-Salazar, J., Morales-Luna, M., "Enhanced photocatalytic activity of TiO₂-ZnO thin films deposited by dc reactive magnetron sputtering." *Ceram. Int.*, 2017, 43, 8831–8838.
- 0.3
0.4
- 0.5 39. Kamaruddin, S. A., Chan, K. Y., Yow, H. K., Zainizan Sahdan, M., Saim, H., Knipp, D., "Zinc oxide films prepared by sol-gel spin coating technique." *Appl. Phys. A Mater. Sci. Process*, 2011, 104, 263–268.
- 0.6
0.7
- 0.8 40. Ravishankar, S., Balu, A. R., Anbarasi, M., Nagarethinam, V. S., "Influence of precursor molar concentration on the structural, morphological, optical and electrical properties of PbS thin films deposited by spray pyrolysis technique using perfume atomizer." *Optik. (Stuttg.)*, 2015, 126, 2550–2555.
- 0.9
1.0
1.1
- 1.2 41. Kouidri, Nabila, Rahmane, Saâd, "Effect of Cobalt Chloride Concentration on Structural, Optical and Electrical Properties of Co₃O₄ Thin Films Deposited by Pneumatic Spray." *Journal of New Technology and Materials*, 2020, 10, 56–62.
- 1.3
1.4
- 1.5 42. Sbeta, M., Atilgan, A., Atli, A., Yildiz, A., "Influence of the spin acceleration time on the properties of ZnO:Ga thin films deposited by sol-gel method." *J. Solgel. Sci. Technol.*, 2018, 86, 513–520.
- 1.6
1.7
- 1.8 43. Shaikh, A. A., Waikar, M. R., Sonkawade, R. G., "Effect of different precursors on electrochemical properties of manganese oxide thin films prepared by SILAR method." *Synth. Met.*, 2019, 247, 1–9.
- 1.9
2.0
- 2.1 44. Guettaf Temam, E., Djani, F., Rahmane, S., Ben Temam, H., Gasmi, B., "Photocatalytic activity of Al/Ni doped TiO₂ films synthesized by sol-gel method: Dependence on thickness and crystal growth of photocatalysts." *Surfaces and Interfaces*, 2022, 31, 077-102.
- 2.2
2.3
2.4
- 2.5 45. Xiaohong, W., Wei, Q., Li, L., Yun, G., Zhaoyang, X., "Photocatalytic property of nanostructured Fe³⁺-doped Bi₂O₃ films." *Catal. Commun.*, 2009, 10, 600–604.
- 2.6
- 2.7 46. Qin, W., Qi, J., Wu, X., "Photocatalytic property of Cu²⁺-doped Bi₂O₃ films under visible light prepared by the sol gel method." *Vacuum*, 2014, 3–6.
- 2.8
- 2.9 47. Mokrani, N., Guettaf Temam, E., Barkat, H., Ben Temam, H., Rahmane, S., Althamthami, M., "Boosting photocatalytic stability: hydrophilic Sr-doped ZnO thin films prepared via the SILAR method for enhanced performance over multiple cycles." *Phys. Scr.*, 2024, 99, 094-095.
- 3.0
3.1
3.2
- 3.3 48. Jothibas, M., Manoharan, C., Dhanapandian, S., Jeyakumar, S. J., "Influence of precursor concentration on sprayed In₂O₃ thin films." *Asian Journal of Chemistry*, 2013, 25.
- 3.4
3.5
- 3.6 49. Althamthami, M., Temam, G., Hachmi, E. I., Temam, H. Ben, Hasan, G. G., Gasmi, B., Hasan, G., Rahmane, S., "Tailor-made Tenorite (CuO) Interface Films for Enhanced Photocatalysis: An Improved Dip-Coating Approach with Enhanced Surface Topography and Hydrophobicity." 2023, 1.
- 3.7
3.8
3.9

- 040 50. Lu, H., Hao, Q., Chen, T., Zhang, L., Chen, D., Ma, C., Yao, W., Zhu, Y., "A high-
041 performance Bi₂O₃/Bi₂SiO₅ p-n heterojunction photocatalyst induced by phase
042 transition of Bi₂O₃." *Appl. Catal. B*, 2018, 237, 59–67.
- 043 51. Begum, S., Ahmaruzzaman, M., "Green Synthesis of SnO₂ Nanoparticles loaded on
044 Activated Carbon and its Application as Photocatalyst in the Degradation of Alizarin
045 Red S Dye." *Mater. Today Proc.*, 2018, 5, 2314–2320.
- 046 52. Islam, M. R., Rahman, M., Farhad, S. F. U., Podder, J., "Structural, optical and
047 photocatalysis properties of sol–gel deposited Al-doped ZnO thin films." *Surfaces and
048 Interfaces*, 2019, 16, 120–126.
- 049 53. Li, J., Guo, J., Zhang, J., Sun, Z., Gao, J., "Surface etching and photodeposition
050 nanostructures core-shell Cu₂O@CuO-Ag with S-scheme heterojunction for high
051 efficiency photocatalysis." *Surfaces and Interfaces*, 2022, 34, 102-308.
- 052 54. Tornabene, F., Triantafyllou, T., Teklemariam Gaim, Y., Mekides Yimanuh, S., Girmay
053 Kidanu, Z., "Enhanced Photocatalytic Degradation of Amoxicillin with Mn-Doped
054 Cu₂O under Sunlight Irradiation." *Journal of Composites Science*, 2022, 6, 317.
- 055 55. Balarak, D., Mengelizadeh, N., Rajiv, P., Chandrika, K., "Photocatalytic degradation of
056 amoxicillin from aqueous solutions by titanium dioxide nanoparticles loaded on
057 graphene oxide." *Environmental Science and Pollution Research*, 2021, 28, 49743–
058 49754.
- 059 56. Kusuma, K. B., Manju, M., Ravikumar, C. R., Dileepkumar, V. G., Kumar, A. N.,
060 Santosh, M. S., Murthy, H. C. A., Gurushantha, K., "Probe Sonicated Synthesis of
061 Bismuth Oxide (Bi₂O₃): Photocatalytic Application and Electrochemical Sensing of
062 Ascorbic Acid and Lead." *J. Nanomater.*, 2022.
- 063 57. Zahid, A. H., Han, Q., Jia, X., Li, S., Hangjia, H., Liu, H., "Highly stable 3D multilayered
064 nanoparticles-based β-Bi₂O₃ hierarchitectre with enhanced photocatalytic activity."
065 *Opt. Mater. (Amst.)*, 2020, 109, 110-389.
- 066 58. Abu-Dief, A. M., Mohamed, W. S., "α-Bi₂O₃ nanorods: synthesis, characterization and
067 UV-photocatalytic activity." *Mater. Res. Express*, 2017, 4, 035-039.
- 068 59. Perez-Mezcua, D., Bretos, I., Jiménez, R., Ricote, J., Jiménez-Rioboó, R. J., da Silva, C.
069 G., Chateigner, D., Fuentes-Cobas, L., Sirera, R., Calzada, M. L., "Photochemical
070 solution deposition of β-Bi₂O₃ thin films." *J. Solgel. Sci. Technol.*, 2017, 81, 355–361.
- 071 60. Wu, S., Xie, Y., Zhang, X., Huang, Z., Liu, Y., Fang, M., Wu, X., Min, X., "In situ synthesis
072 of adsorptive β-Bi₂O₃/BiOBr photocatalyst with enhanced degradation efficiency." *J.
073 Mater. Res.*, 2019, 34, 3450–3461.
- 074 61. Ravi Dhas, C., Venkatesh, R., David Kirubakaran, D., Princy Merlin, J., Subramanian, B.,
075 Moses Ezhil Raj, A., "Electrochemical sensing of glucose and photocatalytic
076 performance of porous Co₃O₄ films by nebulizer spray technique." *Mater. Chem.
077 Phys.*, 2017, 186, 561–573.

- 078 62. Althamthami, M., Guettaf Temam, E., Ben Temam, H., Hasan, G. G., Malfi, N.,
079 "Influence of hole-scavenger and different withdrawn speeds on photocatalytic
080 activity of Co₃O₄ thin films under sunlight irradiation." *Ceram. Int.*, 2022, 48, 31570–
081 31578.
- 082 63. Xu, L., Su, J., Zheng, G., Zhang, L., "Enhanced photocatalytic performance of porous
083 ZnO thin films by CuO nanoparticles surface modification." *Materials Science and
084 Engineering: B*, 2019, 248, 114-405.
- 085 64. Mrabet, C., Jaballah, R., Mahdhi, N., Boukhachem, A., Amlouk, M., "CuO-ZnO
086 nanocomposites-based thin films: Characterization, physical properties and sunlight
087 photocatalytic degradation of organic pollutants." *J. Alloys. Compd.*, 2023, 968, 172-
088 252.
- 089 65. Habibi, M. H., Shojaee, E., "Synthesis of a heterojunction CoTiO₃/Co₃O₄ nano-
090 composite thin film with superior photocatalytic activity and reusability: Effect of
091 calcination temperature on phase transformation and effect of oxidants on enhanced
092 degradation of Indo Light Blue dye." *Spectrochim. Acta A Mol Biomol. Spectrosc.*,
093 2020, 229, 117-796.
- 094

Impress